RSC Advances

ROYAL SOCIETY OF CHEMISTRY

www.rsc.org/advances

Graphical abstract

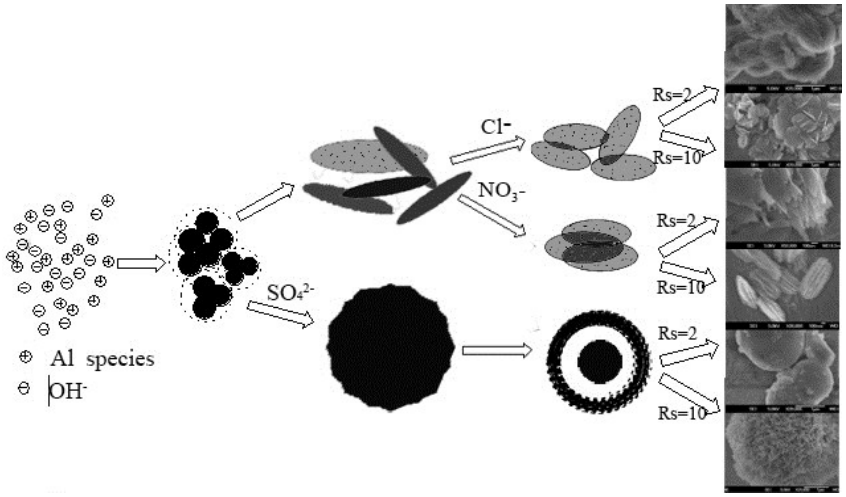

Hierarchical γ-Al_2O_3 nanostructures with tunable morphologies including irregular nanoflake assemblies, hami melon-like nanoflake assemblies, flower-like ellipsoid, hollow core/shell and hollow microsphere, and enhanced adsorption performance towards phenol and CO_2 were synthesized for the first time by a facial one-pot template-free hydrothermal method and sequential calcination route using aluminum sulfate, aluminum chloride and aluminum nitrate as aluminium precursors, respectively and thiourea as precipitating agent.

Cite this: DOI: 10.1039/c0xx00000x

www.rsc.org/xxxxxx

PAPER

Template-free synthesis of hierarchical γ-Al_2O_3 nanostructures and their adsorption affinity toward phenol and CO_2

Weiquan Cai,*[a] Yuzhen Hu,[a] Jiaguo Yu,[b] Wenguang Wang,[b] Jiabin Zhou[c] and Mietek Jaroniec[d]

Received (in XXX, XXX) Xth XXXXXXXXX 20XX, Accepted Xth XXXXXXXXX 20XX

DOI: 10.1039/b000000x

Hierarchical γ-Al_2O_3 nanostructures with tuneable morphologies including irregular nanoflake assemblies, melon-like nanoflake assemblies, flower-like ellipsoids, hollow core/shell and hollow microspheres were successfully synthesized for the first time via a facile template-free hydrothermal method using aluminium sulfate, aluminium chloride and aluminium nitrate as aluminium sources, respectively, and thiourea as precipitating agent. Their phase structures, morphologies, textural and basic properties were characterized by X-ray diffraction (XRD), scanning electron microscopy (SEM), transmission electron microscopy (TEM), selected area electron diffraction (SAED), N_2 adsorption-desorption and CO_2 temperature programmed desorption (CO_2-TPD). The results indicate that thiourea, type of anions in the aluminium sources and the molar ratio of thiourea to Al^{3+} play an essential role in the formation of the aforementioned hierarchical γ-Al_2O_3. A growth mechanism of chemically induced self-transformation followed by cooperative self-assembly to form hierarchical nanostructures was proposed. In contrast, the γ-Al_2O_3 hollow core/shell microspheres with average pore size of 14.3 nm obtained from aluminium sulfate shows the highest adsorption capacity of 28 mg/g towards phenol at 25 °C. However, the hierarchical γ-Al_2O_3 obtained from aluminium chloride and aluminium nitrate with smaller average pore size of 5.2 nm and 5.4 nm, respectively, are more effective for CO_2 capture. This study provides new insights into the design and synthesis of hierarchical nanostructures for environmentally relevant applications.

Introduction

Alumina is of great interest for a variety of applications because of its unique optical, electronic, catalytic, adsorption and biomedical properties[1-4]. Therefore, the synthesis of alumina with controllablly physicochemical properties is an important topic of ongoing research[5-8]. Among various alumina materials, hierarchical γ-Al_2O_3 nanostructures have attracted especial attention because their micro-sized overall structures consist of nano-sized low-dimensional building blocks, making them more attractive for a variety of applications[9-10].

γ-Al_2O_3 is usually obtained *via* dehydration of boehmite at 400-700 °C, depending on the nature of the precursors used. During calcination, boehmite undergoes an isomorphous transformation to nanocrystalline γ-Al_2O_3 without altering its morphology; thus, extensive efforts have been made to control the morphology of boehmite[11]. Formation of hierarchical nanostructures is widely considered as a self-assembly process involving self-aggregation of various building blocks such as nanoparticles (0D), nanofibers, nanowires and nanoribbons (1D), nanosheets and nanoflakes (2D) into higher level structures[12]. Hydrothermal/solvothermal routes allow tuning of boehmite morphology via soft/hard template or structure-directing agent such as sodium tartrate, cetyltrimethylammonium bromide, tetrabutylammonium bromide, block copolymers and polyvinylpyrrolidone, which can direct the crystal growth to afford different morphologies[6,13-15]. Up to now, various hierarchical boehmite/γ-Al_2O_3, such as nonwovens[16], ellipsoidal flower-like, rotor-like, carambola-like and leaf-like micro/nanoarchitectures[17], flower-like or spindle-like nanostructures[18], cantaloupe-like structures constructed by close packing of nanorods[19], flower-like structures composed of nanoplates[20], core-corona nanostructures[21] and hollow and self-encapsulated microspheres assembled from nanosheets and naonrods[22-23] have been reported.

In our previous works[6,9,24], hierarchical boehmite hollow core-shell and hollow microspheres, spindle-like and nanorod-like mesoporous nanostructures were synthesized *via* sodium tartrate, and SO_4^{2-} mediated phase self-transformation processes; these hierarchical alumina structures show good adsorption affinity toward Congo red and phenol contained in aqueous solutions. However, a facile hydrothermal synthesis of hierarchical alumina with controllable morphology and multifunctional adsorption performance is still lacking. Herein, we report for the first time a facile template-free hydrothermal synthesis of various hierarchical γ-Al_2O_3 nanostructures using inexpensive inorganic aluminum salts as alumina precursors and thiourea as precipitant. The effects of aluminum source, molar ratio of thiourea to Al^{3+} and hydrothermal time on the physiochemical properties of the resulting aluminas were studied. A series of time-dependent

experiments was conducted to explain the mechanism of assembly of hollow microspheres from nanoflakes. Moreover, the performance of the hierarchical γ-Al_2O_3 nanostructures and γ-Al_2O_3 obtained from commercial boehmite for phenol and CO_2 adsorption was comparatively studied.

Experimental section

Synthesis of alumina samples

The reagents were all analytical grade supplied by Shanghai Chemical Reagent Ltd. (P. R. China) and used as received without further purification. And distilled water was used. In a typical synthesis, 5.38 g of thiourea ($CS(NH_2)_2$) was added into 70 ml of $Al_2(SO_4)_3$ solution (the concentration of Al^{3+} was 0.1 mol·L^{-1}) under vigorous stirring for 30 min at 25 °C. Then the resulting solution was transferred into a 100 mL Teflon autoclave, and kept at 180 °C for 3 h before cooling to 25 °C. The final precipitate was collected *via* vacuum filtration, washed with distilled water three times and subsequently one time with anhydrous alcohol, and dried in a vacuum oven at 80 °C for 12 h. The as-synthesized hydrated alumina was calcined at 550 °C for 4 h at a heating rate of 1.5 °C·min^{-1} to prepare hierarchical γ-Al_2O_3. Other syntheses were analogous to the above one except using $AlCl_3$ or $Al(NO_3)_3$ instead of $Al_2(SO_4)_3$ and varying the molar ratio of thiourea to Al^{3+} (Rs) from 2 to 10. The final samples were labelled, starting with a prefix of A referring to γ-Al_2O_3 or P referring to its precursor followed by the type of aluminum precursors (s, c and n refering to $Al_2(SO_4)_3$, $AlCl_3$ and $Al(NO_3)_3$, respectively), and ending with Rs. For example, A-s-10 denotes γ-Al_2O_3 synthesized from $Al_2(SO_4)_3$ with Rs of 10. Furthermore, the calcined sample of a commercial boehmite (SB) obtained from the Research Institute of Petroleum Processing, China Petroleum Chemical Co., Ltd was labelled as A-SB.

Characterization

Phase structures of the samples studied were analyzed on a Rigaku D/max-RA X-ray diffractometer (Rigaku, Japan) with Cu-Kα radiation (λ=1.5406 Å) at a scan rate (2θ) of 0.05 °·s-1. Morphology analysis was performed by using an S4800 field-emission scanning electron microscopy (FE-SEM, Hitachi, Japan) with an acceleration voltage of 5 kV. Transmission electron microscopy (TEM) and selected area electron diffraction (SAED) analysis were performed using a Tecnai G2 20 microscope at an accelerating voltage of 200 kV. The N_2 adsorption-desorption isotherms were recorded on a Micromeritics ASAP 2020 gas adsorption apparatus. The BET surface areas of the samples were determined by a multipoint BET method using the adsorption data in the relative pressure (P/P_0) range of 0.05-0.2. All the samples were degassed at 120 °C prior to N_2 adsorption measurement. Desorption isotherms were used to determine the pore size distribution (PSD) by the Barret-Joyner-Halenda method. The N_2 adsorption volume at P/P_0 of 0.998 was used to determine the pore volume and the average pore size[25].

Measurements of phenol adsorption

Adsorption of phenol was measured by adding 75 mg of the sample into 150 mL of phenol solution with a concentration of 100 mg·L^{-1} at an initial pH of 9.5 under vigorous stirring at room temperature. Analytical sample was taken from the suspension after desirable adsorption time and separated by microfiltration. The residual phenol concentration was analyzed by using a UV-vis spectrophotometer (UV-2550, Shimadzu, Japan). The characteristic absorption of phenol around 285 nm was chosen to monitor the adsorption process.

Measurements of CO_2 adsorption

Adsorption of CO_2 was measured using ultra high purity CO_2 in a pressure range of 0-0.1 MPa at 25 °C on a Tri Star Ⅱ 3020 analyzer (Micromeritics Instrument Corporation). All the samples were degassed at 300 °C for 4 h before analysis. The temperature programmed desorption of CO_2 (CO_2-TPD) was performed on a Chemisorb 2720 analyzer using N_2 as carrier gas with a flow rate of 30 mL·min^{-1}. Prior to the CO_2 adsorption, all the samples were heated to 550 °C, then cooled to 25 °C and exposed to CO_2 at a flow rate of 30 mL·min^{-1} for 30 min. Desorption of CO_2 proceeded by heating at a rate of 10 °C·min^{-1} up to 550 °C.

Results and discussion

Structural properties

The XRD patterns of the samples obtained before and after calcination are shown in Fig. 1, and indicate that P-c-10 and P-n-10 feature the same phase structure with diffraction peaks characteristic for boehmite (JCPDS No. 21-1307). No impurities were detected, indicating high purity of the samples. However, the XRD pattern of the P-s-10 synthesized from $Al_2(SO_4)_3$ shows also additional diffraction peaks at 2θ=17.7, 25.4, 29.6 and 49.0 ° indicating that SO_4^{2-}, NH_4^+ and Al^{3+} coexist in the form of a complex salt, which can be identified as ammonioalunite (JCPDS

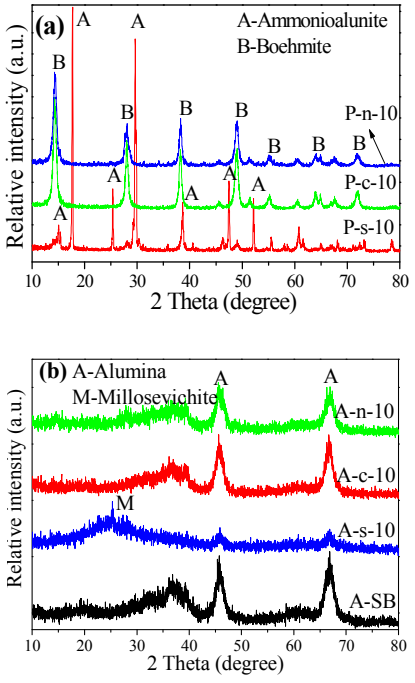

Fig.1 XRD patterns of the aluminas before (a) and after (b) calcination synthesized from different aluminum precursors at Rs=10

No. 42-1430). In contrast, Cl^- and NO_3^- have no obvious effect on the phase structure, and boehmite is the only phase. This difference may be due to the facts that SO_4^{2-} is able to bridge

polymeric hydroxylated aluminum complexes and has higher precipitating capacity than those of Cl^- and NO_3^-[11,26].

Fig. 1b shows that all the reflection peaks of A-c-10 and A-n-10 are in a good agreement with cubic γ-Al_2O_3 (JCPDS No. 10-0425), indicating that the complete conversion of P-c-10 and P-n-10 into γ-Al_2O_3 occured *via* calcination. The broad diffraction peaks reveal their nanosized nature. However, in comparison to the γ-Al_2O_3 synthesized from $AlCl_3$ and $Al(NO_3)_3$, and to the A-SB obtained by calcination of from commercial boehmite, the XRD pattern of the A-s-10 sample synthesized from $Al_2(SO_4)_3$ shows not only very weak diffraction peaks at 2θ=45.9 and 67.0 ° of γ-Al_2O_3, but also indicates the presence of another phase, which is indexed as millosevichite (JCPDS No. 42-1428) at 2θ=25.3°.

Morphologies

Morphologies and microstructures of the calcined samples were characterized by SEM, TEM and SAED, as shown in Fig. 2. It shows that the A-s-10 sample consists of well-defined hollow core/shell microspheres assembled from densely organized 2D nanoflakes. Inset in Fig. 2a shows that the microspheres have diameters of ca. 3.5-4 μm, and the SAED pattern of the shell with rings and spots illustrates its polycrystalline nature. The diffraction rings are not well resolved, suggesting low crystallinity of this sample[27]. Fig. 2b shows that A-c-10 consists of bundles of several twisted nanoflakes with lengths of ca. 800 nm and widths of ca. 150 nm. While A-n-10 consists of monodispersed and well-defined melon-like nanoflake assemblies. Fig. 2b and c also show that the SAED patterns of the two samples exhibit typical single crystalline diffraction peaks[27].

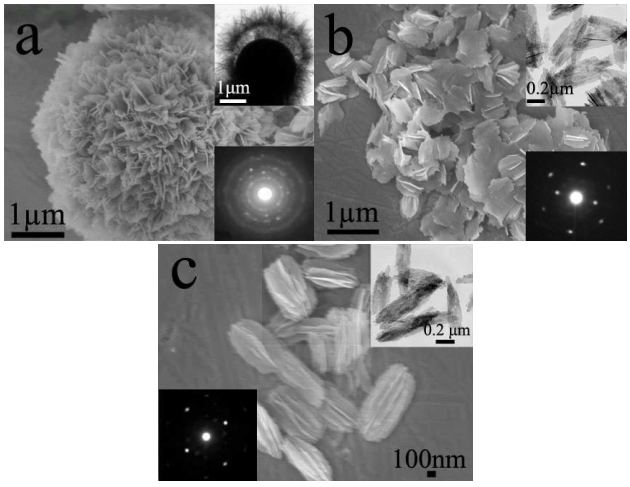

Fig.2 SEM, TEM and SEAD images of the aluminas synthesized from different aluminum precursors at Rs=10: (a) A-s-10, (b) A-c-10 and (c) A-n-10

The SEM images of the hierarchical alumina obtained from different aluminum precursors at low Rs = 2 were also shown in supporting information. Fig. S1 and S2 show that A-s-2 synthesized from $Al_2(SO_4)_3$ consists of asymmetrical amorphous alumina microspheres. However, A-c-2 synthesized from $AlCl_3$ is in the form of uniform ellipsoidal flower-like γ-Al_2O_3 nanostructures with a size of ca.1.5 μm in length, and A-n-2 is mainly in the form of stacked lamellar-like γ-Al_2O_3 nanostructures. The above images indicate that the morphology of the aluminas can be effectively tuned by adjusting both the proper type of anion in the aluminum precursor and the molar ratio of thiourea to Al^{3+}.

Textural properties

The textural properties of the samples were further analyzed by N_2 adsorption-desorption. Fig. 3a shows that the isotherm for A-s-10 is type IV, which is characteristic of mesoporous materials[25]. While the isotherms for A-c-10 and A-n-10 are type II with a small H3 hysteresis loop in the P/P_0 range of 0.7~1.0, suggesting the presence of large mesopores and small macropores formed during aggregation of plate-like particles[28]. Fig. 3b shows that their PSD curves support the aforementioned discussion. The PSD curve for A-s-10 shows a maximum around ca. 18.2 nm, and in the cases of A-c-10 and A-n-10 the corresponding maximum is around 48.7 nm and 44.7 nm, respectively.

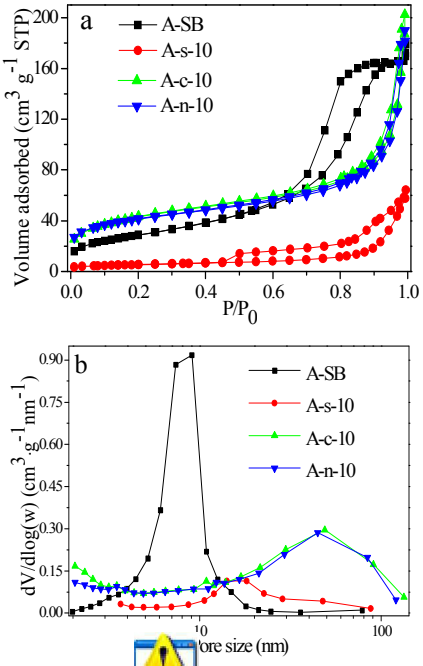

Fig.3 N_2 adsorption-deso[illegible]otherms (a) and their corresponding PSD curves (b) for th[illegible] obtained from different aluminum precursors

The pore structure parameters of the samples were listed in Table 1. Textural properties of the A-c-10 and A-n-10 samples

Table 1 Pore structure parameters of the hierarchical aluminas prepared from different aluminium precursors and γ-Al_2O_3 obtained by calcination of commercial boehmite

Sample	Specific surface area /m^2 g^{-1}	Pore volume /cm^3 g^{-1}	Average pore size /nm
A-SB	104.8	0.26	9.8
A-s-10	18.8	0.07	14.3
A-c-10	145.4	0.20	5.2
A-n-10	145.1	0.20	5.4

synthesized from $AlCl_3$ and $Al(NO_3)_3$, respectively, are very similar. Furthermore, their specific surface areas and pore volumes are much higher, and their average pore sizes are much lower than that evaluated for the A-s-10 sample prepared from

$Al_2(SO_4)_3$, indicating that NO_3^- and Cl^- except SO_4^{2-} affect similarly the textural properties of the samples studied.

Formation mechanism

To investigate the formation process of the various hierarchical alumina nanostructures, the time-dependent evolution of the boehmite hollow microspheres obtained from $Al_2(SO_4)_3$ at Rs=10 was elucidated by SEM, TEM and XRD (Fig. 4) as an example.

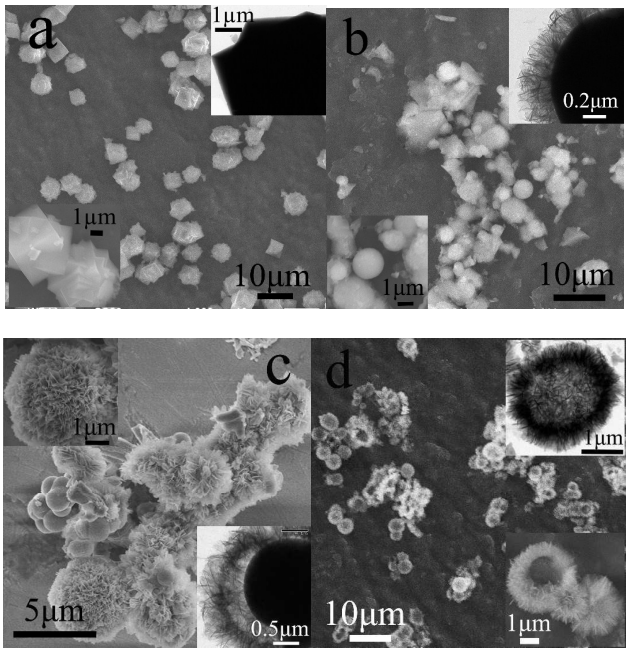

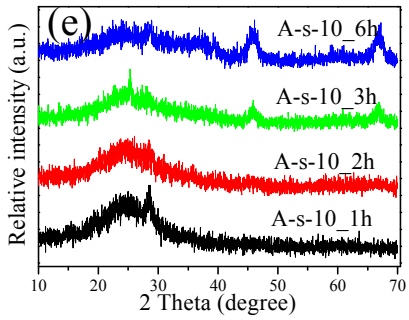

Fig.4 SEM and TEM images of the samples synthesized from $Al_2(SO_4)_3$ by varying the hydrothermal time: (a) 1, (b) 2, (c) 3, (d) 6 h and their corresponding XRD patterns after calcination (e)

Fig. 4a and 4e show that the irregularly amorphous microparticles with clear edges and corners, having diameters of ca. 5-7 μm, were obtained after 1 h. With further increase of the hydrothermal synthesis time to 2 h, a spontaneous phase transformation occurs, and the aforementioned edges and corners dissolves quickly. As aresult, a large number of nanoflakes form epitaxially on the surface of the microspheres (Fig. 4b).

When the hydrothermal time was increased to 3 h, the progressive dissolution of the metastable microspheres results in the weakly crystalline core-shell hollow structures (Fig. 4c and 4e). A further increase in the hydrothermal time to 6 h results in the complete dissolution of the solid cores, and in the formation of the well-defined hollow spheres with diameter of ca. 2.5 μm and higher crystallinity (Fig. 4d and 4e).

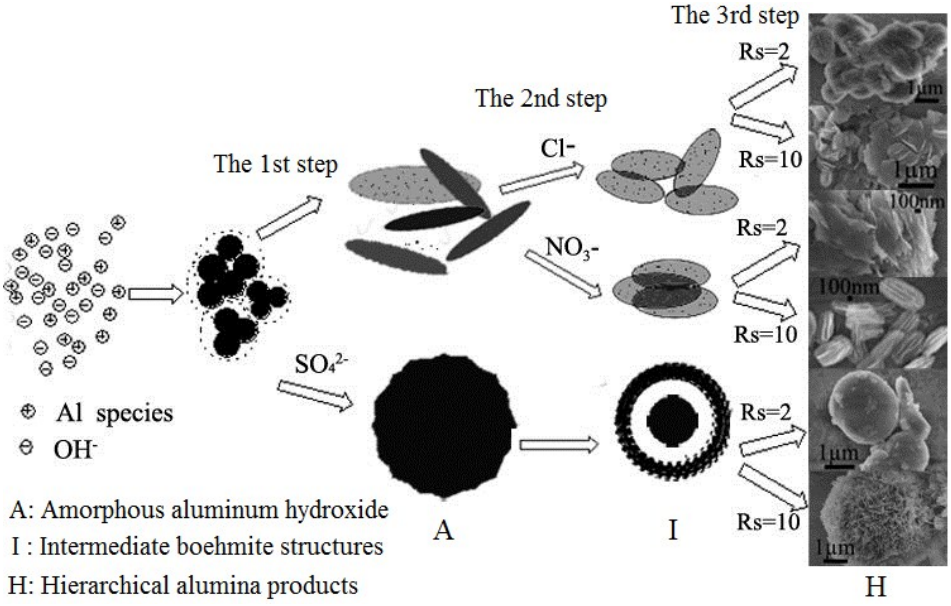

Fig.5 Schematic illustration of the morphology evolution of the hierarchical alumina nanostructures

Based on the time-dependent evolution result, the formation mechanism of the hierarchical architectures can be envisioned as a three-stage process: (1) formation and aggregation of amorphous particles, (2) nucleation stage with localized Ostwald ripening, involving the chemically induced self-transformation associated with preferential dissolution of the particle interior, and (3) preferential growth via cooperative self-assembly, as shown in Fig. 5[11,17,29-30]. First, thiourea is a bidentate ligand, C=S bonds in thiourea are easily attacked by oxygen atoms of H_2O, and thiourea begins to decompose to CO_2, NH_3 and H_2S at elevated temperatures according to the following reaction[31-34]:

$$H_2N-CS-NH_2+2H_2O \xrightarrow{\Delta} CO_2+2NH_3+H_2S \quad (1)$$

$$NH_3+H_2O \rightleftharpoons NH_3\cdot H_2O \rightleftharpoons NH_4^+ + OH^- \quad (2)$$

With the pH of the solution increaseing uniformly, sequential hydrolysis and polycondensation of Al^{3+} kinetically favours deposition of irregularly spheroidal amorphous aluminum hydroxide particles according to the following reactions[13]:

$$Al^{3+} \xrightarrow{OH^-} [Al(OH)]^{2+} \xrightarrow{OH^-} [Al(OH)]^{+} \xrightarrow{OH^-} Al(OH)_3(amorphous) \quad (3)$$

$$Al(OH)_3(amorphous) \rightarrow \gamma - AlOOH + H_2O \quad (4)$$

Secondly, an in-situ phase transformation of the metastable amorphous particles located on the outermost surface, especially on the edges, serves as the starting point for the subsequent dissolution-recrystallization process (equation 4), resulting in a void space between the loosely packed exterior and the closely packed interior[32]. The boehmite crystallites prefer to grow on the edges of the already existing crystallites along the main crystallographic [001] axis to form nanoflakes/nanoplates with higher thermodynamic stability under appropriate basic hydrothermal conditions[13,35-36]. The nanoflakes is a layered structure with an octahedral arrangement within the lamellae, and hydroxyl ions hold the lamellae together through hydrogen bonding[37]. Then, the progressive dissolution and redistribution of the matter from the interior to the exterior proceeds, resulting in the formation of the hollow structures assembled from the oriented cross-linked nanoflakes. Finally, γ-Al_2O_3 can be obtained by calcination of boehmite, which undergoes an isomorphous transformation (equation 5).

$$2\gamma - AlOOH \rightarrow \gamma - Al_2O_3 + H_2O \quad (5)$$

It is known that thiourea can be use as a complexant to form ZnS hollow spheres, and benefits the oriented growth of the final hierarchical structures assembled from building blocks[32,38]. The gradual decomposition rate of thiourea accelerates with increasing the reaction time and temperature, and the content of S^{2-} and its migration rate accordingly increase. This may accelerate the growth of nano-crystallites to a larger size at a higher rate, and results in morphology change of the final product[31-33]. Also, thiourea as a surface modified agent, can prevent agglomeration of the nanoparticles. In comparsion with the boehmite hollow structures obtained from $Al_2(SO_4)_3$[39], the assembly of nanoflakes obtained using $AlCl_3$ and $Al(NO_3)_3$ as aluminum sources, respectively, results in flower-like ellipsoidal nanostructures (Fig. 2). The observed difference may be due to the following reasons. Firstly, SO_4^{2-} has higher affinity to bridge polymeric hydroxylated aluminum complexes than NO_3^- and Cl^-, and thus the hydrothermal system in the presence of SO_4^{2-} favours the formation of spheroidal particles[11]. Secondly, as an electroneutral ligand, thiourea forms complexes with Al^{3+} through Al-S coordination bonding, which not only adjusts the precipitation rate, but also promotes the oriented growth of the hierarchical structures assembled from building blocks[31-33,40].

Adsorption of phenol and CO_2

Recently, a considerable attention has been paid to removal of pollutants by using thermally and chemically stable sorbents such as alumina and related oxyhydroxides[8,41,42]. Hierarchical nanomaterials are promising for environmental remediation for their unique micro-/nanostructures can prevent aggregation and their high surface area enhances the accessibility of adsorbates to reactive sites[43]. Phenol is a widespread and highly toxic compound, which is a by product in some industrial processes and difficult to degrade biologically[44]. Furthermore, CO_2 is the main source causing green-house effect. As it was shown above, different precursors $Al_2(SO_4)_3$, $AlCl_3$ and $Al(NO_3)_3$ afford alumina samples with different properties. Therefore, it is worthy to explore how these differences, induced by different anions in the aforementioned precursors, affect adsorption of phenol and CO_2. Fig. 6 shows data for phenol adsorption on the aluminas (also see Fig. S3 with error bars). Among them, A-s-10 adsorbs the highest amount of phenol (28.0 $mg \cdot g^{-1}$) at a contact time of 60 h, which is notably higher than 16.1 $mg \cdot g^{-1}$ adsorbed by A-c-10, and 23.2 $mg \cdot g^{-1}$ by A-n-10, respectively. However, the commercial A-SB sample adsorbs only 20.5 $mg \cdot g^{-1}$ of phenol. Furthermore, adsorption of phenol on A-s-10 can be approximatively divided into 3 stages. Initially (the first 2 h period), phenol was immediately adsorbed reaching the amount of 17.5 $mg \cdot g^{-1}$. Next, between 2~48 h, phenol was slowly adsorbed resulting in an additional adsorption of 9.5 $mg \cdot g^{-1}$. Finally, between 48~60 h, an almost complete saturation was achieved resulting in the adsorption capacity of 28.0 $mg \cdot g^{-1}$.

Furthermore, the static adsorption kinetics and adsorption capacity of phenol on A-s-10 is respectively faster and higher

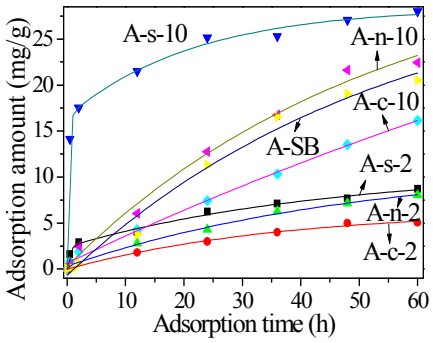

Fig.6 Adsorption amounts of phenol on the hierarchical aluminas prepared from different aluminum precursors at different molar ratio of thiourea to Al^{3+}

than in the case of other aluminas such as spindle-like γ-Al_2O_3 (21.0 $mg \cdot g^{-1}$ after 6 h)[9], dodecyl sodium sulfate-modified neutral alumina (3.75 $mg \cdot g^{-1}$)[45], and the activated alumina particulates of 63-150 mm without any affinity for phenol adsorption[46], whereas still lower than that of the hierarchical micro-nano porous carbon and the commercial activated carbon (241.2 $mg \cdot g^{-1}$ and 220.4 $mg \cdot g^{-1}$ at 100min, respectively)[47]. Previous studies showed that phenol uptake is a combined effect of physisorption which is the dispersive interactions of the phenol with the basal planes, and chemisorption which takes place between the OH group of phenol and the functional groups on the adsorbent surface[48]. Since phenol is a relatively small molecule consisting of benzene ring with one H substituted with OH group, it can accommodate even in micropores and interact well with the γ-Al_2O_3 surface[49]. The highest adsorption of phenol on A-s-10, which has the lowest surface area among the samples, may be ascribed to its unique hollow structure and surface properties that are favourable for attracting phenol molecules. Note that the formation of alumina structures is markedly influenced by the release rate and amount of OH^- in the hydrothermal system, which depend mainly on the

initial concentration of thiourea and Al^{3+}. As a result, the hierarchical γ-Al_2O_3 samples synthesized at various Rs values (for instance, 2 and 10) may possess different concentrations of active sites (e.g., surface hydroxyls), which affect adsorption of phenol molecules. Data for phenol adsorption also suggest that the samples synthesized at low Rs values possess much less active sites responsible for phenol adsorption.

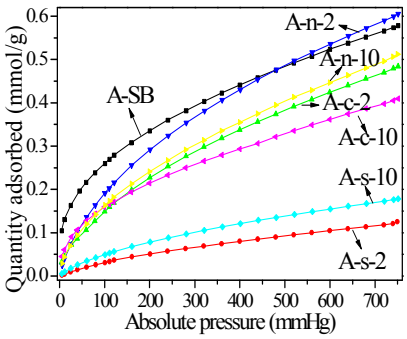

Fig.7 Adsorption isotherms of CO_2 on hierarchical aluminas synthesized from different aluminum precursors

CO_2 adsorption isotherms measured on the aluminas at 25 °C are shown in Fig. 7. It shows that the adsorption amounts at 750 mmHg for the aluminas obtained from $AlCl_3$ and $Al(NO_3)_3$ are higher than that of the sample prepared from $Al_2(SO_4)_3$ at a molar ratio of thiourea to Al^{3+} of 2 and 10, respectively. Especially, A-n-2 synthesized from $Al(NO_3)_3$ shows the highest adsorption amount of 0.6 mmol·g^{-1}, which is notably higher than 0.1 mmol·g^{-1} of A-s-2 prepared from $Al_2(SO_4)_3$. Since CO_2 adsorption amount is larger on the samples with higher surface area, A-n-2 shows higher CO_2 uptake[50,51]. Also, basic properties may enhance CO_2 adsorption (see below).

The basic properties of the selected alumina samples were further investigated by CO_2-TPD analysis. As shown in Fig. 8, both A-n-10 and A-c-10 have a distinct and broad desorption peak, which starts at about 25 °C, and reaches maximum value at 65 and 56 °C, respectively ascribable to weakly adsorbed CO_2 species, indicating that CO_2 molecules weakly interact with the samples surface via physisorption. Such a low-temperature desorption due to physisorption is an advantage of A-n-10 and A-c-10 when they are employed as adsorbents for their easy desorption. However, the desorption peak of A-s-10 starts at much higher temperature, exceeding 420 °C, which can be assigned to strongly adsorbed CO_2 species via chemisorption[52-54]. In contrast, for the commercial γ-Al_2O_3, three CO_2 desorption peak at 86 °C, 283 °C and 620 °C ascribable to weakly adsorbed CO_2 species, strongly adsorbed CO_2 species and carbonate formation respectively, were detected[55]. In view of this phenomenon, the commercial γ-Al_2O_3 is inferior to the prepared alumina samples which are more suitable for CO_2 capture. It is remarkably noticed that there is a full saturation in the case of phenol and little saturation in case of CO_2 for A-s-10 (see Fig.6 and Fig.7), and thus A-s-10 shows more selective adsorption affinity towards phenol versus CO_2. This remarkably adsorption difference may be due to the following reasons: the weak crystallinity with polar surface, the big average pore size of 14.3 nm and the hollow core/shell structure of A-s-10 are beneficial to adsorbing the weak polar phenol molecule with larger molecular size and weaker acidity; however, its above physicochemical properties, poor physisorption sites and rich chemisorptions sites restrain its adsorption at 25 °C toward non-polar CO_2 with small molecular size and certain acidity. Furthermore, as an alumina, A-s-10 possesses negative surface charge in aqueous solution due to accumulation of hydroxyl (OH−) ions on its surface[56], and this is also beneficial to adsorbing phenol molecule versus CO_2.

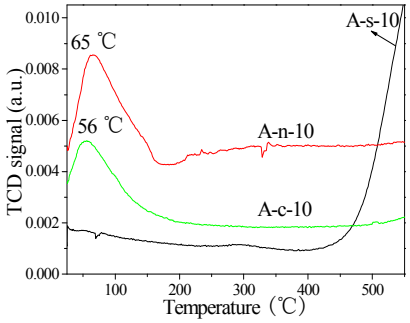

Fig.8 CO_2-TPD patterns of the hierarchical aluminas synthesized from different aluminum precursors

Conclusion

A variety of hierarchical γ-Al_2O_3 samples with controlled morphologies including irregular nanoflake assemblies, melon-like nanoflake assemblies, flower-like ellipsoids, hollow core/shell and hollow microspheres have been synthesized by a facile thiourea-assisted homogeneous hydrothermal precipitation method. Evolution of their morphologies and structural transformations can be easily manipulated by varying the type of anion (SO_4^{2-}, Cl^- and NO_3^-) in the aluminium precursor, the molar ratio of thiourea to Al^{3+} and the hydrothermal time. The chemically induced self-transformation and followed self-assembly resulting from the synergistic effect of thiourea and the anion assisting the aforementioned processes are the main driving forces for the formation of these hierarchical γ-Al_2O_3 structures. Adsorption studies show that the γ-Al_2O_3 hollow core/shell microspheres synthesized from $Al_2(SO_4)_3$ performs very well in the case of phenol adsorption, while those prepared from $AlCl_3$ and $Al(NO_3)_3$ exhibit higher CO_2 uptake at ambient conditions. In the case of phenol adsorption the concentration of active sites seems to be more important than the surface area. However, the latter is essential to CO_2 adsorption. The as-synthesized hierarchical γ-Al_2O_3 structures with controllable morphologies and adsorption properties should be attractive materials for various applications including adsorption, separation and catalysis.

Acknowledgements

This work was financially supported by the National Natural Science Foundation of China (51272201, 21476179 and 21277108), Program for New Century Excellent Talents in University of the Ministry of Education (NCET-13-0942), Wuhan Youth Chenguang Program of Science and Technology (2013070104010002), Fundamental Research Funds for the Central Universities of Wuhan University of Technology (2013-II-014) and the State Key Laboratory of Advanced Technology

for Materials Synthesis and Processing, Wuhan University of Technology (2013-KF-5).

Notes and references

[a]*State Key Laboratory of Silicate Materials for Architectures, School of Chemistry, Chemical Engineering & Life Sciences, Wuhan University of Technology, 205 Luoshi Road, Wuhan 430070, P. R. China*
[b]*State Key Laboratory of Advanced Technology for Material Synthesis and Processing, Wuhan University of Technology, 205 Luoshi Road, Wuhan 430070, P. R. China*
[c]*School of Resources and Environmental Engineering, Wuhan University of Technology, 122 Luoshi Road, Wuhan 430070, P. R. China*
[d]*Department of Chemistry and Biochemistry, Kent State University, Kent 44242, Ohio, USA*
[*]Corresponding author. fax: +86-27-87859019;Tel.: +86-27-87859019; *E-mail address*: caiwq@whut.edu.cn

† Electronic supplementary information (ESI) available: one figure showing SEM images of the hierarchical alumina samples obtained from different precursors at Rs=2, and one figure showing the XRD patterns of the hierarchical alumina samples after calcination obtained from different aluminum precursors.

1 Z. Liu and C. Lv, *RSC ADV.*, 2014, **4**, 10221.
2 J. Yu, Z. S. Li, Q. Liu, J. Wang, H. Wei, M. Zhang and L. H. Liu, *RSC ADV.*, 2013, **3**, 6621.
3 M. Benítez-Guerrero, L. A. Pérez-Maqueda, P. E. Sánchez-Jiménez and J. Pascual-Cosp, *Micropor. Mesopor. Mater.*, 2014, **185**, 167.
4 W. Q. Cai, J. G. Yu and S. Mann, *Micropor. Mesopor. Mater.*, 2009, **122**, 42.
5 S. Lan, N. Guo, L. Liu, X. Wu, L. Li and S. Gan, *Appl. Surf. Sci.*, 2013, **283**, 1032.
6 W. Q. Cai, J. G. Yu, B. Cheng, B. L. Su and M. Jaroniec, *J. Phys. Chem. C*, 2009, **113**, 14739.
7 C. C. Liu, J. L. Li, K. Y. Liew, J. J. Zhu and M. R. bin Nordin, *RSC ADV.*, 2012, **2**, 8352.
8 W. Q. Cai, J. G. Yu, C. Anand, A. Vinu and M. Jaroniec, *Chem. Mater.*, 2011, **23**, 1147.
9 W. Q. Cai, J. G. Yu and M. Jaroniec, *J. Mater. Chem.*, 2010, **20**, 4587.
10 J. R. Ge, K. J. Deng, W. Q. Cai, J. G. Yu, X. Q. Liu and J. B. Zhou, *J. Colloid Interface Sci.*, 2013, **401**, 34.
11 W. Q. Cai, J. G. Yu, S. H. Gu and M. Jaroniec, *Cryst. Growth Des.*, 2010, **10**, 3977.
12 Y. D. Yin and D. Talapin, *Chem. Soc. Rev.*, 2013, **42**, 2484.
13 X. Y. Chen, H. S. Huh and S. W. Lee, *Nanotechnology*, 2007, **18**, 285608 (5pp).
14 P. F. Fulvio, R. I. Brosey and M. Jaroniec, *Appl. Mater. Inter.*, 2010, **2**, 588.
15 Y. Q. Wang, G. Z. Wang, H. Q. Wang, W. P. Cai, C. H. Liang and L. D. Zhang, *Nanotechnology*, 2009, **20**, 155604 (6pp).
16 S. Ghosh and M. K. Naskar, *RSC ADV.*, 2013, **3**, 4207.
17 H. Liang, H. X. Yang, J. J. Wei, Z. J. Yang and Y. Z. Yang, *CrystEngComm*, 2011, **13**, 2445.
18 Y. L. Feng, W. C. Lu, L. M. Zhang, X. H. Bao, B. H. Yue, L. Yong and X. F. Shang, *Cryst. Growth Des.*, 2008, **8**, 1426.
19 L. M. Zhang, W. C. Lu, L. M. Yan, Y. L. Feng, X. H. Bao, J. P. Ni, X. F. Shang and Y. Lv, *Micropor. Mesopor. Mater.*, 2009, **119**, 208.
20 G. C. Li, Y. Q. Liu and C. G. Liu, *Micropor. Mesopor. Mater.*, 2013, **167**, 137.
21 C. Wang, S. Z. Huang, L. Wang, Z. Deng, J. Jin, J. Liu, L. H. Chen, X. F. Zheng, Y. Li and B. L. Su, *RSC ADV.*, 2013, **3**, 1699.
22 W. Q. Cai, S. G. Chen, J. G. Yu, Y. Z. Hu, C. X. Dang and S. H. Ma, *Mater. Chem. Phys.*, 2013, **138**, 167.
23 M. Li, Z. Si, X. Wu, D. Weng and F. Kang, *J. Colloid Interface Sci.*, 2014, **417**, 369.
24 W. Q. Cai, Y. Z. Hu, J. Chen, G. X. Zhang and T. Xia, *CrystEngComm*, 2012, **14**, 972.
25 K. S. W. Sing, D. H. Everett, R. A. W. Haul, L. Moscou, R. A. Pierotti, J. Rouquerol and T. Siemieniewska, *Pure Appl. Chem.*, 1985, **57**, 603.
26 R. W. Hicks and T. J. Pinnavaia, *Chem. Mater.*, 2003, **15**, 78.
27 P. Bai, P. P. Wu, Z. F. Yan and X. S. Zhao, *J. Mater. Chem.*, 2009, **19**, 1554.
28 G. Leofanti, M. Padovan, G. Tozzola and B. Venturelli, *Catal. Today*, 1998, **41**, 207.
29 X. W. Lou, L. A. Archer and Z. C. Yang, *Adv. Mater.*, 2008, **20**, 3987.
30 L. S. Zhong, J. S. Hu, A. M. Cao, Q. Liu, W. G. Song and L. J. Wan, *Chem. Mater.*, 2007, **19**, 1648.
31 Z. Obrenovića, M. Milanovićc, R. R. Djenadićd, I. Stijepovićc, K. P. Giannakopoulose, M. Perušića and L. M. Nikolićc, *Ceram. Int.*, 2011, **37**, 3253.
32 X. B. He and L. Gao, *J. Phys. Chem. C*, 2009, **113**, 10981.
33 J. G. Yu, S. W. Liu and M. H. Zhou, *J. Phys. Chem. C*, 2008, **112**, 2050.
34 R. Zamiri, H. A. Ahangar, A. Zakaria, G. Zamiri, H. R. Bahari, G. P. C. Drummen, *J. Nanopart. Res.*, 2014, **16**, 2333.
35 S. W. Liu and J. G. Yu, *J. Solid State Chem.*, 2008, **181**, 1048.
36 T. B. He, L. Xiang and S. L. Zhu, *CrystEngComm.*, 2009, **11**, 1338.
37 Y. X. Lin, W. P. Cai, H. He, X. B. Wang, G. Z. Wang, *RSC Adv.*, 2012, **2**, 1769
38 T. J. Yan, L. P. Li, G. S. Li, *Res. Chem. Intermediat.*, 2011, **37**, 297.
39 X. Y. Chen, X. Wang, Z. H. Wang, X. G. Yang, Y. T. Qian, *Cryst. Growth Des.* 2005, **5**, 347.
40 X. X. Yu, J. G. Yu, B. Cheng and B. B. Huang, *Chem. Eur. J.*, 2009, **15**, 6731.
41 W. Q. Cai, L. J. Tan, J. G. Yu, M. Jaroniec, X.Q. Liu, B. Cheng and F. Verpoort, *Chem. Eng. J.*, 2014, **239**, 207.
42 A. -M. Pierre-Louis, D. B. Hausner, N. Bhandari, W. Li, J. Kim, J. D. Kubicki and D. Strongin, *J. Colloid Interface Sci.*, 2013, **400**, 1.
43 J. S. Hu, L. S. Zhong, W. G. Song and L. J. Wan, *Adv. Mater.*, 2008, **20**, 2977.
44 C. L. He, J. H. Huang, J. B. Liu, L. B. Deng and K. L. Huang, *J. Appl. Polym. Sci.*, 2011, **119**, 1435.
45 A. Adak and A. Pal. *Desalin. Water Treat.*, 2009, **6**, 269.
46 N. Roostaei, F. H. Tezel, *J. Env. Man.*, 2004, **70**, 157
47 C. B. Liu, Z. G. Chen, C. Y. Ni, F. Chen, C. Gu, Y. Cao, Z. Y. Wu, P. Li, *Rare Metals*, 2012, **31**, 582.
48 I. I. Salame and T. J. Bandosz, *J. Colloid Interface Sci.*, 2003, **264**, 307.
49 S. D. Chakarova-Käck, Ø. Borck, E. Schröder and B. I. Lundqvist, *Phys. Rev. B*, 2006, **74**, 155402.
50 H. Hattori, *Chem. Rev.*, 1995, **95**, 537.
51 D. M. D'Alessandro, B. Smit and J. R. Long, *Angew. Chem. Int. Ed.*, 2010, **49**, 6058.
52 W. Q. Cai, J. G. Yu and M. Jaroniec, *J. Mater. Chem.*, 2011, **21**, 9066.
53 H. Hattori. J. Heidberg and B. Redlich, *Surf. Sci.*, 1996, **368**, 140.
54 M. K. R. Reddy, Z. P. Xu, G. Q. Lu and J. C. D. D. Costa, *Ind. Eng. Chem. Res.*, 2006, **45**, 7504.
55 H. N. Li, L. Zhang, H. X. Dai, H. He, *Inorg. Chem.*, 2009, **48**, 4421.
56 M. R. Karim, M. A. Rahman, M. A. J. Miah1, H. Ahmad, M. Yanagisawa, M. Ito, Open Colloid.Sci., 2011, **4**, 32.